

DENKI-SEIKO (Electric Furnace Steel), vol. 71 (2000), No. 2, p. 119 - 129

Paper

Effect of Si Content on the Machinability of Hot Working Die Steels

Toshimitsu Fujii and Yukinori Matsuda

1. Preface

Hot working die steels containing 5% Cr such as JIS SKD61 are usually used with 42 to 50 HRC hardness after hardened and tempered. In recent years high performance steels featuring low Si and high Mo content have been developed because of findings of those feature's effectiveness to higher toughness and heat check resistance¹⁾. These steels have been commercialized in particular for die-cast molds with design faces^{2), 3)}.

However the wider they were used, the more problem of less machinability than conventional steel like SKD61 has been reported. Therefore countermeasures are desired. Studies on the machinability against Si content for annealed 5% Cr steels (85 – 96 HRB)⁴⁾ or hardened and tempered 0.3C-4Cr-1.5Mo-0.6V-Ni steels (43 HRC)⁵⁾ have been investigated. As the result of those studies, machinability decrease along with decrease of Si content have been clarified, although the mechanism behind the phenomenon has been unexplained well enough.

Moreover recently "Direct Milling" which enables elimination of rough machining of annealed materials by milling directly hardened and tempered steels have been widely applied for the purpose of cost or lead time reduction in hot working die steels.^{6), 7)} This "Direct Milling" have already been applied to 50 HRC material area⁶⁾. Therefore machinability of hardened and tempered steels rather than annealed ones and higher hardness steels among hardened and tempered ones tend to be more important. However as previously mentioned available reports on Si content and machinability for hot working die steels are limited to relatively low hardness ones, less than 43 HRC.^{4), 5)} There are no reports on the effect of Si content on the machinability of hard steel near upper limit of usage area.

Therefore in this study using conventional 5%Cr-3%Mo steel as high performance steel, the effect of Si content on the machinability of hot working die steels have been investigated as well as cutting mechanism change by Si addition.

2. Test conditions

2.1 Specimen

Table 1 shows chemical compositions of specimens. Five steels containing Si from 0.05% to 1.5% have been prepared while main components have remained as Fe-0.35%C-0.6%Mn-5%Cr-3%Mo-0.85%V. They were melted by Vacuum Induction Heated furnace and casted to 150 kg of ingots. Ingots were heated to 1503 K, forged to 68 mm squared billets and annealed.

Table 1. Chemical compositions of test steels

steel	C	Si	Mn	Cr	Mo	V
A	0.33	0.05	0.60	5.53	3.01	0.83
B	0.33	0.15	0.60	5.53	3.00	0.84
C	0.33	0.29	0.60	5.55	3.01	0.84
D	0.34	0.99	0.60	5.55	3.01	0.84
E	0.34	1.52	0.60	5.54	3.01	0.84

Specimens for microscopic examination, end-mill machining, turning and high temperature tensile tests were taken from annealed billets, machined roughly, hardened and tempered and finished before providing them for each testing. All specimens were heated at 1303K for 1.8 ks, quenched in 6 bar of gas before tempered for 3.6 ks twice at 878K for steel A and 883 K for other four steels in order to adjust hardness as 49 ± 1 HRC. Si is well-known additive to increase high temperature softening resistance of steel⁸⁾. This phenomenon was observed in these materials as well since higher Si steel had more secondary hardening amount after tempering. However difference of hardness after tempering according to Si content around tested temperature, 880 K is rather small, and the difference of tempering temperature to acquire the same hardness is as small as 5 K.

2.2 Experimental procedure

(1) Microstructure observation

Microstructure were observed for sections parallel to forging directions. Surfaces of specimens were polished and etched with Nital before optical microscopic observation were taken place. Scanning Electron Microscope (SEM) observation with as-polished specimens were also taken place to investigate the state of carbides precipitation. SEM observation was also carried out for as-quenched samples.

(2) Evaluation of machinability by end-milling

Generally machinability is evaluated by 1) chip processing capacity, 2) cutting resistance, 3) tool life, and 4) machining accuracy⁹⁾. In this study machinability of end-milling cutting which is widely used for mold machining was evaluated by tool life that is usually problematic in actual process. Cutting condition is shown in Table 2. Side-face cutting with 32 mm diameter throw-away end mills were taken place using #40 taper spindle horizontal machining center. Tool life was defined as times when maximum flank face abrasions become $300 \mu\text{m}$ by measuring abrasion amount of carbide tool every certain cutting length. Specimen dimension was 65 mm squared by 200 mm length. Measurement of tool abrasion amount was taken place at cutting length of $2^n \times 100$ mm. Damage state of same carbide tools under every certain cutting distance were observed by SEM to understand damaging process. These observations were taken place for different tools from tool life measurement tools to eliminate effect of treatment of SEM observation on tool life.

Table 2. Cutting conditions for tool life test in end-milling

Diameter of end-mill	$\Phi 32$
Number of tooth	1
Tool grade	M20(Carbide), Non coating
Tool geometry	AEMW19T308ER
Axial depth of cut	4 mm
Radial depth of cut	1 mm
Cutting speed	35.8 m/min
Feed	0.15 mm/tooth
Cutting method	Down cut
Cutting fluid	Dry
Criterion for tool life	Flank wear = 300 μm

(3) Measurement of cutting resistance and cutting temperature

Difference of machinability are often examined by analyzing cutting force or cutting temperature. However since in 3-dimensional cutting, cutting force analysis is very complicated and cutting temperature measurement is extremely difficult for end-mill cutting in machining center, cutting resistance and cutting temperature were measured by two dimensional turning. As shown in Figure 1, by grooving turning test pieces with 65 mm diameter, disk parts with 2 mm in thickness were produced. Table 3 shows the condition of two dimensional turning test. Piezoelectric cutting dynamometer was used to measure cutting resistance. Principal partial force and feed partial force are measurement items and machinability indicators. Cutting mechanism were considered by analyzing cutting forces. Cutting temperature were measured by tool-work thermocouple method as shown in Fig. 1. Thermoelectromotive force generated during turning was measured and temperature was calculated from calibration curve produced by data previously measured using same material combination. Cutting temperature measured by this method are said to be mean temperature between chip-tool contact area¹⁰⁾.

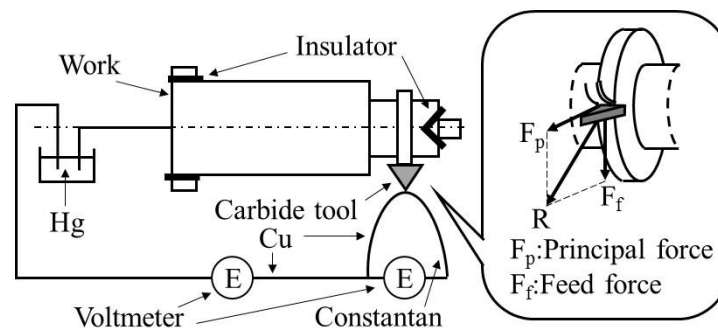


Fig. 1. Measurement method of cutting force and cutting temperature.

Table 3. Cutting conditions for cutting force and cutting temperature measurement in turning

Tool grade	M20(Carbide), Non coating
Tool geometry	TNGA160404
Cutting speed	50 m/min
Feed	0.15 mm/rev.
Width of cut	2 mm
Cutting fluid	Dry

(4) Microstructure observation of chips

It is known that cutting shape was reflected by cutting state difference¹¹⁾. Therefore observation of longitudinal section of chips generated by turning were taken place. After polishing observation face, etching was done by Nital before optical microscopic observation. SEM back scattered image observation of as-polished samples were also taken place and carbide precipitation status was investigated. Moreover in order to confirm oxidation status of chip surface, Transmission Electron Microscope (TEM) observation for sections of chip surface was taken place. Film specimen were taken from chips generated by turning and were prepared using Focused Ion Beam Spattering (FIB) as shown in Figure 2.

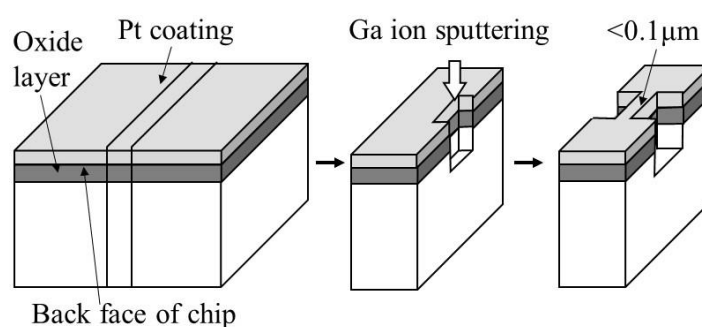


Fig. 2. FIB method to prepare cross-sectional specimens for TEM.

(5) High temperature high speed tensile test

It is known that cutting chips are formed by extremely large plastic deformation in primary shearing stress area and secondary shearing stress area and their strain speed is likely to be in the order of $10^2\text{s} - 10^5/\text{s}$. Therefore Gleeble tensile equipment which enables high speed tensile testing was utilized to perform high temperature tensile test in order to investigate cutting mechanism from high temperature deformation morphology. Geometry of tensile test pieces are 4.5mm in diameter and 25 mm long of parallel part. They were taken from billets so that their axis direction is as same as forging direction. Tensile testing was performed with the speed of 800 mm/s after the temperature was raised to 873 – 1273 K in 100 s and was kept at the testing temperature for 60 s, and deformation load and reduction of area at fracture were measured. The strain speed in this condition was calculated as about 50/s. This value is larger than normal static tensile test, but is smaller than actual cutting deformation.

3. Results and discussion

3.1 Microstructure observation

Optical microscopic observation results of hardened and tempered structure of each sample are in Figure 3. They were all martensitic structures and showed no large differences by Si content.

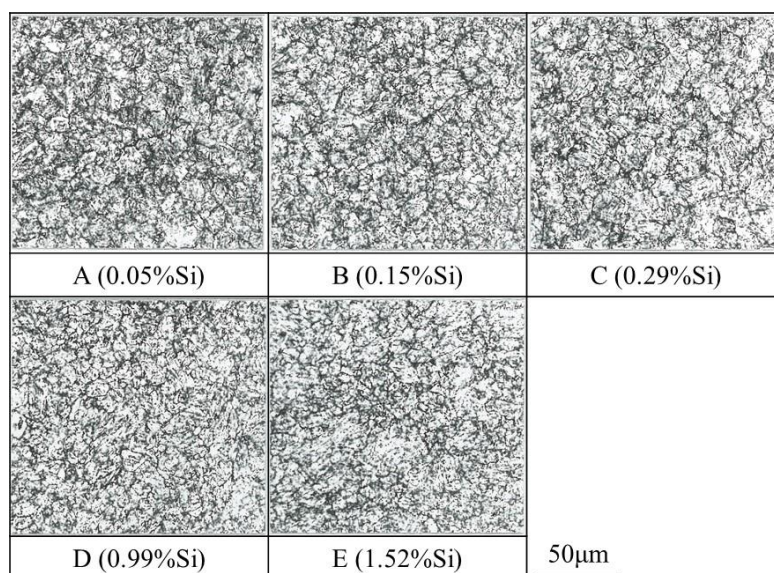


Fig. 3. Microstructures of test specimens.

Figure 4 shows SEM observation results of as-hardened and hardened and tempered steel A, C and E. In SEM observations, back scattered images were used to clarify the differences in carbide compositions. White colored areas and black colored areas were analyzed by Energy Dispersive X-ray Spectroscopy (EDX) and concentration of Mo in white areas and that of V in black area were confirmed, which lead to M_6C carbides and MC carbides respectively. Sizes of M_6C and MC carbides are about $0.5 \mu m$ and the amount of these carbides decreases drastically with decrease of Si content. It is noted that since no large difference was confirmed in the amount of carbides with or without tempering, very fine carbides which precipitate during tempering were not captured by SEM observations. Therefore observed carbides in this study are considered to be residual carbides which had existed during forging and unsolved during hardening.

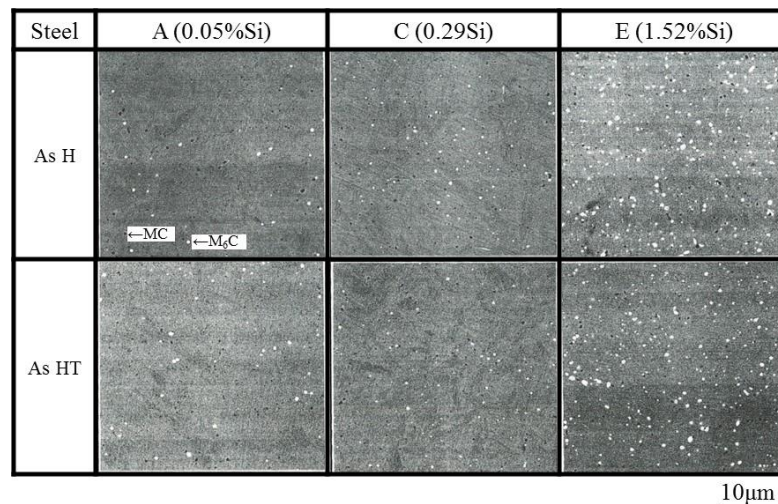


Fig. 4. Back scattering electron images of carbides in hardened specimens and tempered ones.

Now stability of carbides were calculated using thermodynamic equilibrium software, Thermo-Calc. Figure 5 shows equilibrium phase diagram of target composition system with change of Si content. This phase diagram shows decrease of solution temperature of M_6C and MC carbides with decrease of Si content, which explains decrease of residual carbides in low Si steel qualitatively. For example, M_6C carbides do not exist in steel with less than 1% Si content while they do exist in steel with more than 1% Si. Actually not many M_6C carbides were confirmed in low Si steel, thus observation results and calculated phase diagram by Thermo-Calc were matching well. However since production process is not carried out under equilibrium condition, some M_6C carbides remain insignificantly.

From above results, Si has the effect of raising solution temperature of M_6C and MC carbides and with decrease of Si content the solution temperature of M_6C and MC carbides decrease resulting in decrement of carbide amount which remain at hardening treatment.

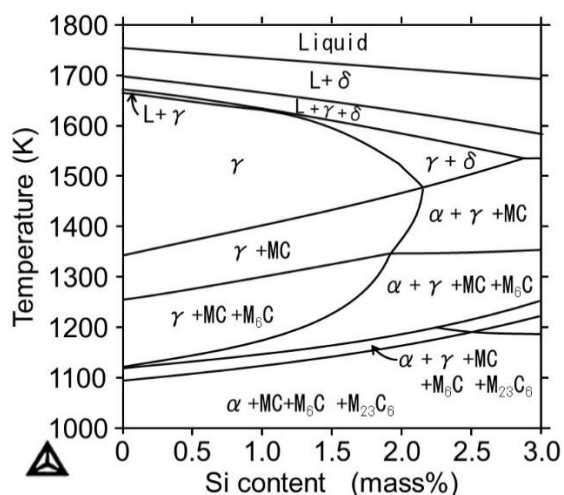


Fig. 5. Vertical section phase diagram of the Fe-0.35%C-Si-0.6%Mn-5.5%Cr-3%Mo-0.85%V system calculated by thermo-calc.

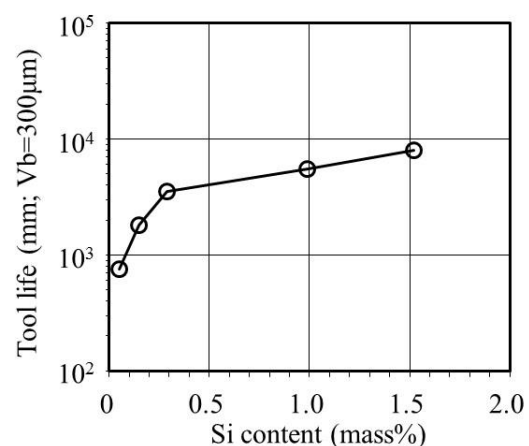


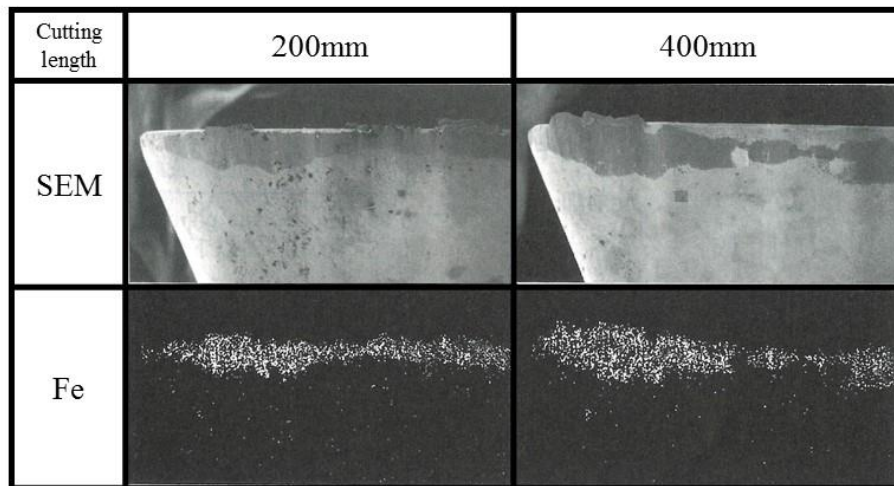
Fig. 6. Effect of Si content on tool life in end-milling.

3.2 Machinability of end-milling

Figure 6 shows the relationship between Si content and tool life in end-milling. Tool life declines with decrease of Si content and the amount of tool life decrease tends to larger in the region where Si content is below 0.3%. It is clarified that, as it has been reported for conventional relatively low hardness material^{4), 5)}, machinability declines with the decrease amount of Si for hardened and tempered hot working die steels with hardness of 49 HRC which is the maximum limit of usage. Moreover, comparing with past reports on the view point of large drop of tool life, in which tool lives decline drastically around less than 0.3 to 0.5% Si^{4), 5)}, this study's result is almost the same.

Figure 7 shows SEM observation results of damaging process of flank face of carbide tools. The lower row of each photo corresponds to characteristic X-ray image of Fe, which explains adhesion of test material. Steel A having low Si content, shows adhesion of material at the cutting length of 200 mm and the adhesion area becomes larger and detachment can be observed at the cutting length of 400 mm. On the other hand steel D having high Si content does not show any adhesion of material at the cutting length of 400 mm and at the cutting length of 800 mm adhesion and detachment can be observed. Therefore the cause of decline in tool lives for low Si material can be considered that the adhesion of material occurs more easily with low Si steel than high Si steel, adhesive wear progresses more rapidly. Besides, although for steel B as well as steel A adhesion of material was observed at the cutting length of 200 mm, for steel C adhesion was not observed at 200 mm length but was observed at 400 mm length. The reason why tool lives drop drastically below 0.3% Si steel is considered to acceleration of adhesion starting timing occurs below around 0.3% Si.

(a) Steel-A (0.05%Si)



(a) Steel-D (0.99%Si)

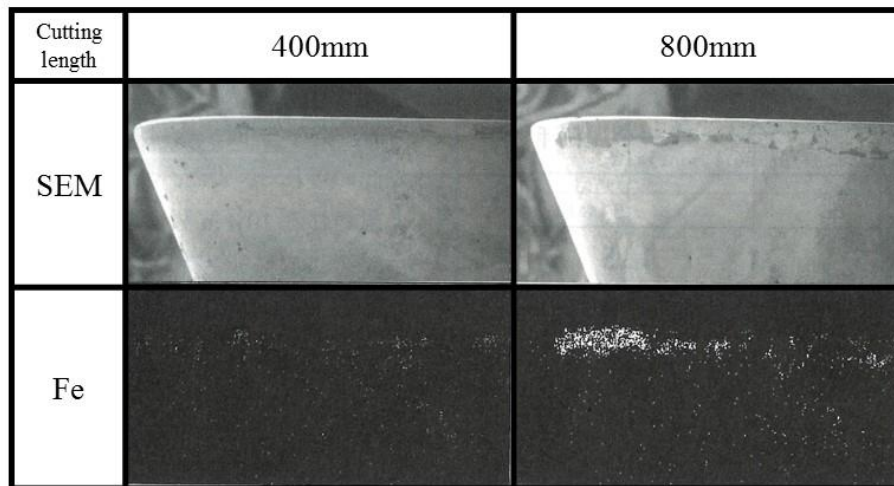


Fig. 7. SEM and characteristic X-ray images of clearance face of carbide tool in end-milling.

3. 3 Results of cutting resistance and cutting temperature measurement

Figure 8 shows the relationship between Si content and cutting resistance in case of turning. All principal partial force, F_p , feeding partial force, F_f and cutting resultant force, R tend to increase with decreasing Si content, so machinability in turning process is supposed to decrease with Si content decrease. The analysis using these results will be discussed in the last section.

Figure 9 shows relationship between Si content and cutting temperature. Cutting temperature reached 915 to 1165 K and increases with decrease in Si content. Temperature difference between steel A and steel E is 250 K, therefore influence of Si on cutting temperature is considered to be significant. Moreover, the color of chips turned to light blue from purple in accordance with decrease of Si content, which proves that the cutting temperature for low Si steel is high¹²⁾. From this result, it is assumed that the cutting temperature tends to rise easily for low Si steel under same cutting conditions. In case of end milling, although cutting mechanism is different, it is also assumed that the cutting temperature is high for low Si steel and adhesive wear tends to occur more easily. A_{C1} transformation temperature of each test material is about 1100 K, and

the cutting temperature of steels with Si content lower than 0.3% seems to be higher than A_{C1} temperature as shown in the phase diagram (Fig. 5). Even though it was not verified yet, adhesion of materials is related to A_{C1} transformation temperature. It is possible to assume that tool life drops drastically below certain Si content because the cutting temperature overtakes A_{C1} transformation temperature.

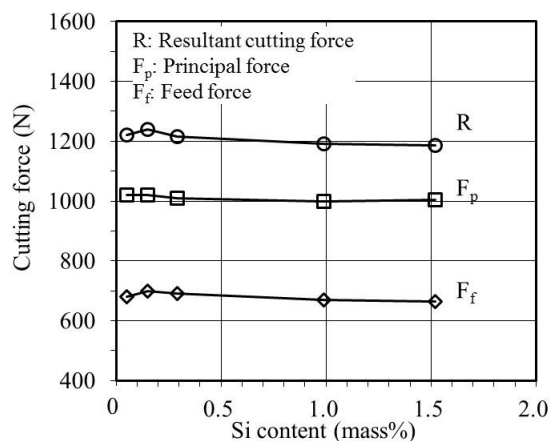


Fig. 8. Effect of Si content on cutting forces in turning.

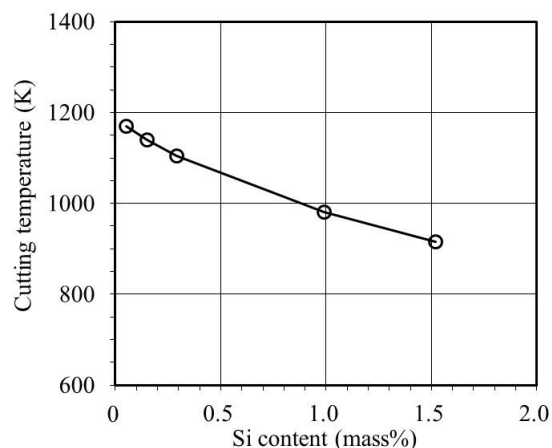


Fig. 9. Effect of Si content on cutting temperature in turning.

3. 4 Microstructure observation of chips

Figure 10 shows optical microscopic observation results for chips generated by turning, and upper side of pictures correspond with back sides of chips (contacting sides to tool's rake face). Chip shape is all flow-type¹¹⁾, and the plastic flow by primary shear deformation can be recognized. Moreover, white layers of about 10 μ m in thickness on surfaces of back sides of chips are formed, which might be caused by thermal effect. Chip shapes and microstructures did not show large differences depending on Si content, therefore cutting states did not seem to be very different.

SEM observation results of chip surfaces are shown in the right column of Fig. 10. They were back scattered images of back sides of chips and the solution of M_6C carbides can be observed in the area below about 10 μ m from the surface. This means that these areas were heated above 1303 K which corresponds to their hardening temperature, and surfaces of back sides of chips can be considered to be heated above 1303 K by friction heat. It is also assumed that, even if it is momentary phenomenon, outermost layer area must be heated to several hundred degree more than average chip-tool contact face temperature. Carbide solution state depends on Si content, and M_6C carbides were hardly observed for steel A – C. As described earlier, this phenomenon can be explained by the fact that solution temperature of carbides are low and the cutting temperature is high in case of low Si steels. White layers which were observed by optical microscopy can be assumed to be transformed structure which was quenched as the result of heated to high temperature and cooled by heat diffusion.

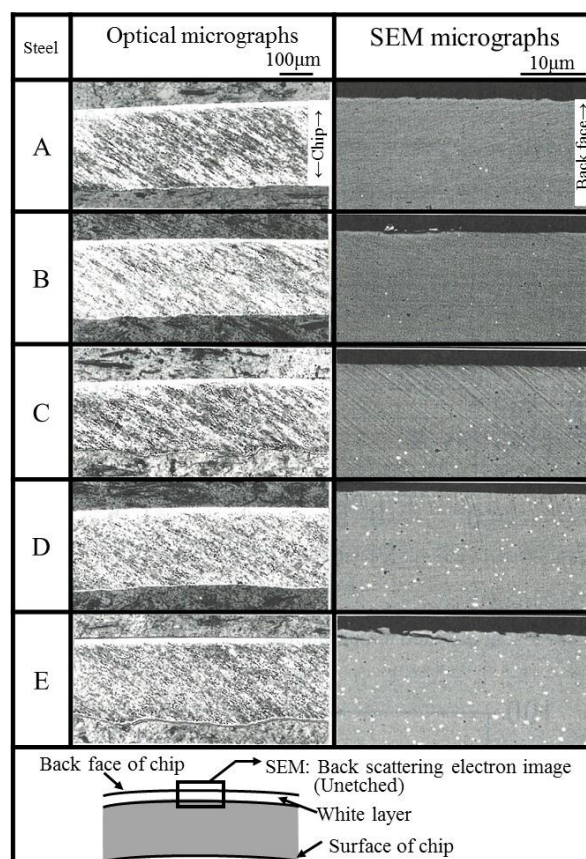


Fig. 10. Microstructure and back scattering electron images of chips in turning.

Okada et al. investigated the relationship between machinability and Si content, by focusing on compositions of oxides which were formed on surfaces of chips. In their report that machinability of 0.3C-4Cr-1.5Mo-0.6V-Ni steel with 43 HRC hardness decrease with decrease of Si content, the difference in machinability is caused by difference in chip deposition property by oxides composition change after performing secondary ion mass spectroscopy analysis, finding out condensation of Cr in oxides of low Si (0.1% Si) steel and their oxides consist of mainly Fe and Cr oxides, while condensation of Cr were not observed in oxides of high Si (1.6% Si) steel and their oxides consist of mainly Fe and Si oxides⁵⁾. Moreover, it is reported that the latter oxides have low melting point and lubrication between chip and tool were enhanced¹³⁾. Therefore chips of steel A and D generated in turning were analyzed after making film sample by FIB method and analyzing oxides compositions by TEM-EDX. Figure 11 shows the result of TEM image and EDX analysis. Both photos show oxide layers of about 0.05 μ m on their surfaces, but no condensation of Cr or Si were observed. Quantitative analysis was performed and the ratio of Fe, Cr and Si in the oxide was nearly the same as processed material. Therefore although oxides formed on low Si steels are mainly consist of Fe and Cr, those formed on high Si steels are not always consist of mainly Fe and Si, and containing the same level of Cr as low Si steels. The reason why our result is different from theirs is not clear, but cutting method difference can be considered. The difference in lubrication effect will be discussed in the last section.

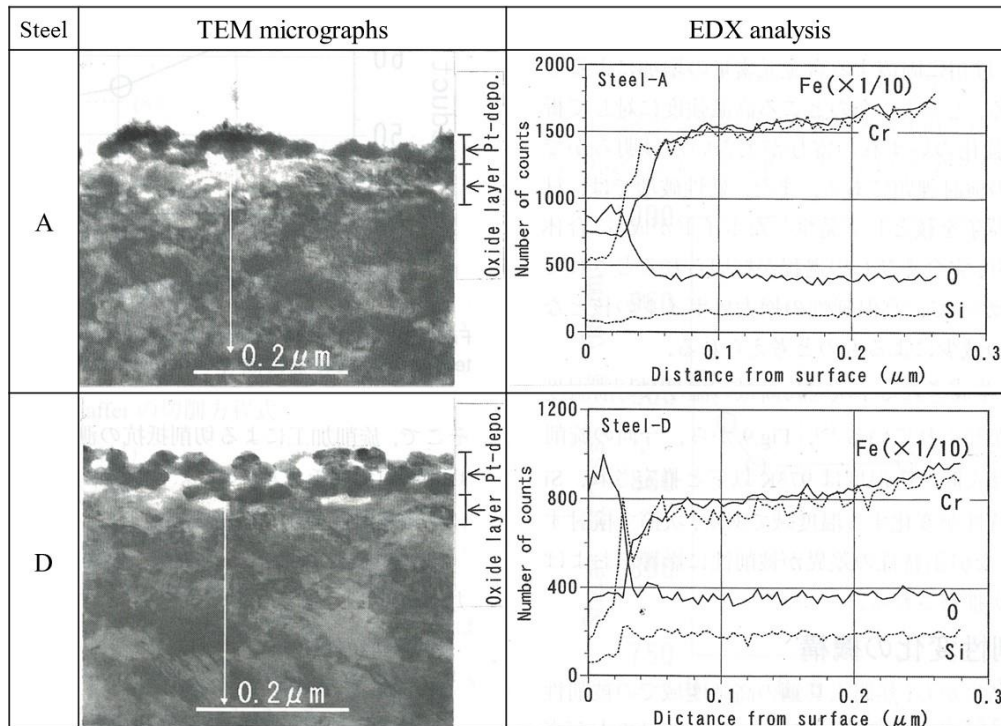


Fig. 11. TEM images of back face of chips and depth profiles of Fe, Si, Cr and O by EDX analysis.

3. 5 High temperature tensile test characteristics

Figure 12 shows the relationship between Si content and maximum deformation stress and Figure 13 shows the relationship between Si content and reduction of areas. Changes in maximum deformation stress and reduction of area are small in 1073 – 1273 K region. This is considered that the temperature is above transformation and composition dependence is small. On the other hand, both maximum deformation stress and reduction of area increase with decrease of Si content at 873 and 973 K. As shown in Fig. 4, amount of residual carbides is smaller in low Si steel, thus the mechanism of change in high temperature tensile test characteristics depending on Si content can be considered as follows. Increase of maximum deformation stress with decrease of Si content is caused by amount increase of fine carbides which precipitate during tempering or by amount increase of alloying elements which dissolve in matrix phase after tempering. However it is not clear which of these elements, precipitation hardening or solution hardening is dominant to high temperature strength. This will be a future assignment. In ductile fracture, voids nucleated by secondary particles in materials grow and combine until completion of necking process¹⁴⁾. Therefore increase of high temperature ductility was due to decrease of retained carbides which can be nuclei of voids.

Moreover, it is known that temperature in primary shear stress area where chips are generated is lower than cutting temperature¹⁵⁾. Temperatures in shear area of turning process in this study are supposed to be lower than 973 K according to Fig. 9. This temperature range is where tensile characteristics changes depending on Si content. These tensile characteristics differences seems to be affect machinability. This will be discussed in the next section.

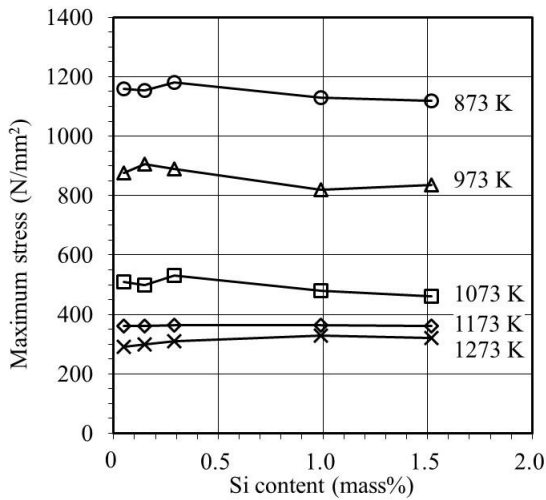


Fig. 12. Effect of Si content on maximum stress in high speed tensile test at elevated temperatures.

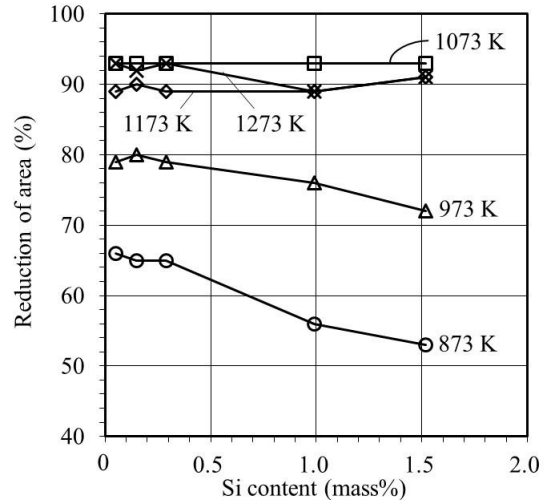


Fig. 13. Effect of Si content on reduction of area in high speed tensile test at elevated temperatures.

3. 6 Mechanism of machinability transition

As a result of these investigation, these facts that machinability of hot working die steels in high hardness state will deteriorate with decrease of Si content and high temperature strength and hot ductility are better for low Si steels were found. Hereinafter mechanism of machinability change with Si content was examined using results of cutting resistance measurement of turning, calculating each cutting partial force by single-shear plane model¹⁶⁾.

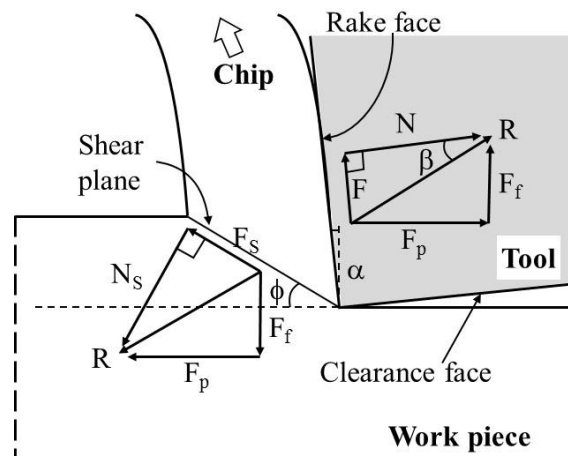


Fig. 14. Two-dimensional cutting model.

Friction force, F and vertical force, N on the rake face of tools occur as shown in Figure 14, and tool rake angle is described as α then following equations can be derived.

$$F = F_p \sin \alpha + F_f \cos \alpha \dots\dots (1)$$

$$N = F_p \cos \alpha - F_f \sin \alpha \dots\dots (2)$$

On the other hand, apparent friction coefficient, μ and cutting shear angle, Φ can be described as

following equations.

$$\mu = \tan \beta = F/N \quad \dots\dots (3)$$

$$\tan \phi = r_c \cos \alpha / (1 - r_c \sin \alpha) \quad \dots\dots (4)$$

Here β shows friction angle, r_c represents cutting ratio and described as following definition.

$$r_c = t/t_c \quad \dots\dots (5)$$

Now focusing on cutting shear faces, cutting resultant force, R can be resolved into shear direction partial force, F_s and vertical force, N_s , while both factors can be described as follows.

$$F_s = F_p \cos \phi - F_f \sin \phi \quad \dots\dots (6)$$

$$N_s = F_p \sin \phi + F_f \cos \phi \quad \dots\dots (7)$$

Shear stress, τ_s can be described using cutting width, b .

$$\tau_s = F_s \sin \phi / (t \cdot b) \quad \dots\dots (8)$$

Moreover, from above equations friction force on rake faces, F and vertical force, N can be derived as follows.

$$F = \tau_s \cdot t \cdot b \sin \beta / \sin \phi \cos(\phi + \beta - \alpha) \quad \dots\dots (9)$$

$$N = \tau_s \cdot t \cdot b \cos \beta / \sin \phi \cos(\phi + \beta - \alpha) \quad \dots\dots (10)$$

In cutting equations that describe the relation between shear face shear angle, ϕ and rake faces friction angle, β , if substitution is made with Lee-shaffer's equation (11) that showed good agreements with this study's results,

$$\phi = \pi/4 - \beta + \alpha \quad \dots\dots (11)$$

following equations can be acquired.

$$N = \sqrt{2} \cdot \tau_s \cdot t \cdot b \cos \beta / \sin(\pi/4 - \beta + \alpha) \quad \dots\dots (12)$$

$$F = \sqrt{2} \cdot \tau_s \cdot t \cdot b \sin \beta / \sin(\pi/4 - \beta + \alpha) \quad \dots\dots (13)$$

Equations (12) and (13) indicate that if t , b and α are known values, by determining either τ_s or β , cutting forces, F or N can be estimated as functions of τ_s or β .

Based on above discussions, Figure 15 shows friction forces, F and vertical forces, N on rake faces of each test material calculated from eq. (1) and (2), as well as change of cutting force when only τ_s decreases keeping β constant as a solid line arrow, and when only friction angle β decreases keeping τ_s constant as broken line arrow. The change of cutting force when Si content is increased compared to steel A is assumed to be close to the solid line arrow. This suggests the change of cutting forces is not brought about by decrease of friction angle or friction coefficient, but by decrease of shear stress.

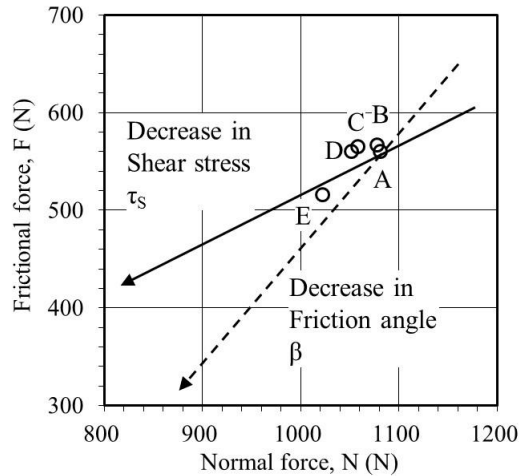


Fig. 15. Influence of change in shear stress and friction angle on normal force and friction force in turning.

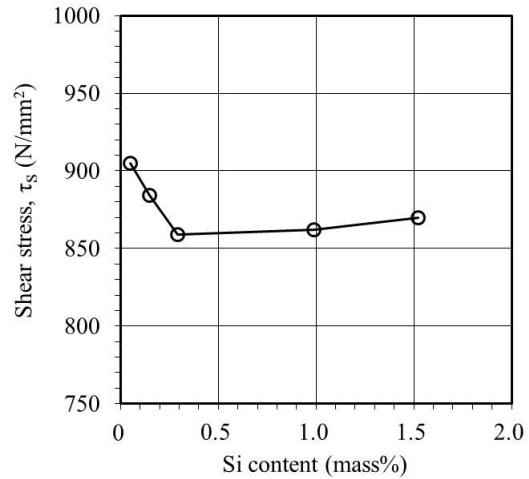


Fig. 16. Effect of Si content on shear stress acting on shear plane in turning.

Therefore, the relationship between Si content and shear stress were calculated using eq. (8). Figure 16 shows those results. Increase of shear stress can be confirmed with decrease of Si content, drastic increase can be seen especially in the region where Si content is less than 0.3%. From above discussion the cutting resistance increase with decrease of Si content can be considered as increase of shear stress. Increase of shear stress originates from high temperature strength judging from the high temperature tensile test result even though strain speed is different. There is another theory that decrease of shear stress comes from higher cutting temperatures for low Si steels. However since temperatures in shearing area are assumed to be lower than 973 K as described previously, shear stress change should be small even if temperatures in shearing area change in case of cutting deformation where strain speed is very high¹⁷⁾. On the other note, the most effective factor on the cutting temperature is known to be shear stresses as M. C. Shaw’s analysis on the cutting temperature¹⁸⁾. Raise in the cutting temperature or acceleration of adhesion wear along with decrease of Si content are also supposed to be the one of causes of increase of high temperature strength.

Moreover, changes of friction angles were investigated. Nakamura et al. have investigated the relationship between cutting resistances and friction angles using JIS SCM420 grade steels with additions of machinability enhancing elements¹⁹⁾. They have reported in the paper that the decrement of ductility in high temperature high speed tensile testing had decreased friction angles and cutting frictions. Therefore, fracture strain, ϵ_f was derived from reduction of area in high temperature high speed tensile testing, ψ , while friction angle β was computed from eq. (3) in order to examine the relationship between them using eq. (14).

$$\epsilon_f = \ln(1/(1 - \psi)) \dots\dots (14)$$

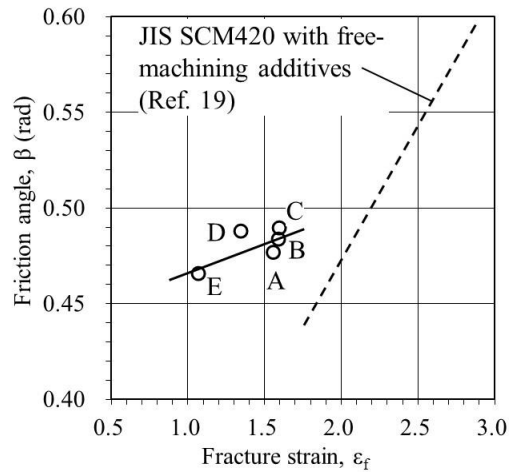
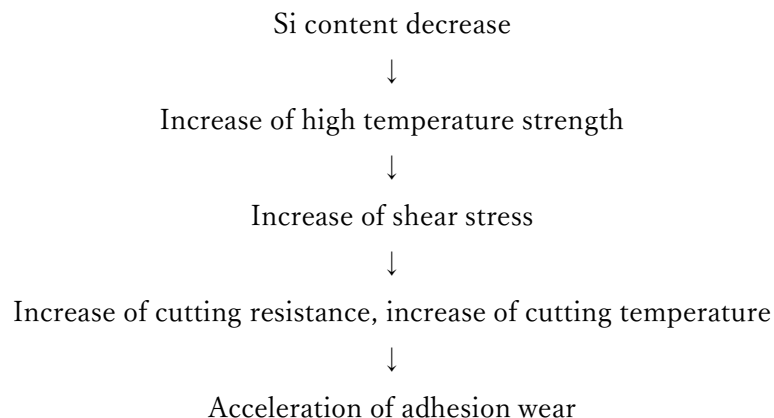


Fig. 17. Relationship between fracture strain in tensile test and friction angle in turning.

Figure 17 shows the relationship between fracture strains and friction angles. Data by Nakamura et al. were added to this figure. Overall tendency, where friction angles decrease with decrement of fracture strains and decrease of high temperature ductility reduces friction angle, shows similarity. However compared with data of Nakamura et al. where they studied effect of machinability enhancing element, the amount of decrease in friction angles depending on the decrease of fracture strains is smaller in this study. This may be the result of small lubricant effect between chip-tool by inclusions. Therefore in materials dealt in this study changes of friction angles are relatively small even though Si content was reduced and the influence of friction angle in other words friction coefficient to the cutting force is considered to be small. This result supports investigation results evaluated in Fig. 15. Even though the lubrication effect increases depending on compositions of oxides, that effect is thought to be small. Lastly, summary of this examination is illustrated by changes of factors related to cutting processes and their relationships in Figure 18. Under the assumption where the result of turning processes can be applied to end-milling processes, the reason why the tool life decreases with decrease of Si content can be considered as follows.



However even though influences are thought to be rather small, changes in high temperature ductility or friction angles were confirmed. It will be necessary to investigate effects of high temperature ductility or friction angles by examining under different hardness levels or different machining conditions.

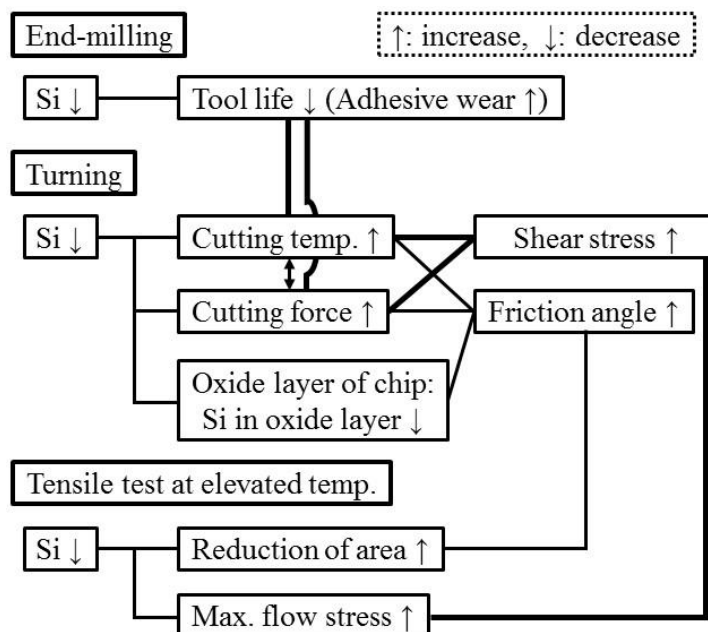


Fig. 18. Changes of factors on machining with decreasing Si content.

4. Conclusion

This study has been carried out to clarify the effect of Si content on machinability of 5%Cr-3%Mo type hot working die steel hardened and tempered to 49 HRC. The results are as follows.

(1) Carbides retained in hardened and tempered specimens are M_6C and MC and the amount of these carbides decrease with the decrease in Si content.

(2) In end-milling, carbide tools exhibit shorter life with decreasing Si content, especially at the range of Si content less than 0.3%. Adhesive wear increases with the decrease in Si content.

(3) In turning by carbide tools, the cutting forces and temperatures rise with decreasing Si content.

(4) High speed tensile test at elevated temperatures reveals that the steels with lower Si content show higher maximum flow stress and larger reduction of area.

(5) By the calculation of turning-cutting forces based on the two-dimensional cutting model, it is found that the decrease in Si content raises the shear stress resulting in the increase of cutting forces. The high shear stress of lower Si steels is considered due to their high strength at elevated temperature.

5. Acknowledgements

Great gratitude has to be expressed to Mr. Masahiro Kawasaki and Mr. Toshiaki Suzuki from Nippon Denshi, who cooperated with us by making film specimens using FIB method and TEM observations.

(Reference)

- 1) K. Sudou: *Denki-Seiko* (Electric Furnace Steel), 60 (1989), p. 367
- 2) T. Okuno: *Tokushukou* (The Special Steel), 46 (1997), No. 7, p. 6

- 3) T. Ogawa: *Tokushukou* (The Special Steel), 46 (1997), No.7, p. 23
- 4) K. Iwamoto: *Denki-Seiko* (Electric Furnace Steel), 64 (1993), p. 191
- 5) T. Sera et al.: *CAMP-ISIJ*, 9 (1996), p. 1404
- 6) M. Fruya et al.: *Kikai Gijutu*, 44 (1996), No. 8, p. 39
- 7) E. Takeoka: *Kikai Gijutu*, 45 (1997), No. 10, p. 22
- 8) T. Nishimura: *Netushori* (Journal of the Japan Society for Heat Treatment), 20(1980), p. 342
- 9) T. Sugita et al.: *Kiso-Sessaku-Kakougaku*, (1984), p. 87 [Kyoritu Shuppan]
- 10) Y. Fujimura: *Jitsuyou-Sessaku-Kakouhou*, (1989), p. 50 [Kyoritu Shuppan]
- 11) E. Shirai: *Sessaku-Kensaku-Kakouhou*, Part I, (1971), p. 8 [Kyoritu Shuppan]
- 12) Y. Fujimura: *Jitsuyou-Sessaku-Kakouhou*, (1989), p. 170 [Kyoritu Shuppan]
- 13) Y. Okada: *Netushori* (Journal of the Japan Society for Heat Treatment), 39 (1999), p. 225
- 14) *Zairyou-Kyoudogaku*, (1986), p. 19 [Nihon Zairyou Gakkai]
- 15) Y. Lee et al.: *Seimitukikai*, 44 (1978), p. 1424
- 16) E. Shirai: *Sessaku-Kensaku-Kakouhou*, Part I, (1971), p. 16 [Kyoritu Shuppan]
- 17) K. Nakayama: *Sessakune-Kakouron*, (1978), p. 109 [Korona Sha]
- 18) E. G. Loewen, M. C. Shaw: *Trans. AMSE*, 76 (1954), p. 217
- 19) S. Abeyama et al.: *Denki-Seiko* (Electric Furnace Steel), 55 (1984), p. 177